2023 American Control Conference (ACC)
San Diego, CA, USA. May 31 - June 2, 2023

Anti-windup Compensation for Stable and Unstable Systems with Quantized and Saturated Inputs*

Christopher M. Richards[1] and Matthew C. Turner[2]

***Abstract*— It is well known that actuator saturation can cause destabilization and degradation in performance; similar problems are faced when actuation is quantized. This paper proposes the design of an anti-windup compensator for systems with actuators that are limited to a *finite* number of quantization levels. This combination of discrete level actuation and saturation poses a unique anti-windup problem that has not yet been solved. To surmount this combined issue, an anti-windup compensator is proposed which provides ultimate-boundedness of the system state within a prescribed region, and also guarantees that the state does not stray outside a larger compact set. A numerical simulation example illustrates the effectiveness on a rigid-body system which inspired this work.**

I. INTRODUCTION

A quantizer maps a continuous-valued signal to a discrete-valued signal [1] and can result from digital-to-analog (D/A) converters, digital sensors and binary actuators, to name a few [2], [3], [4], [5], [6], [7]. The issue of quantization was first discussed in the 1950s by Kalman [8]. However, it was not until the 1990s when Delchamps advocated a direct analysis of the effects of quantization on a system [3]. Quantization can be detrimental to the system response [3], [8], [9]: generally, a system rendered globally asymptotically stable by a control law will not remain so when quantization is introduced [9]. Prior research has addressed logarithmic quantizers where quadratic stability analysis applies [9], [10], [11]. However, this analysis is not applicable for many practical systems with uniform or non-uniform quantization.

Moreover, some mechanical and aerospace systems experience control signals that are subject to both quantization and saturation. For example, the NASA Lunar Pallet Lander utilizes a bank of uni-directional binary actuators that, when used in unison, result in quantized input forces to the vehicle [2]. Likewise, since a finite number of actuators are available, saturation results when thrust demand exceeds the total available thrust. Such a system is typical of a number of practical systems and is the motivation for this work.

The combination of saturation and quantization has not been studied extensively in the literature, with perhaps the most comprehensive treatment given in [12] where conditions were given for state-feedback stabilization of a system subject to input quantization and saturation. Crucially, the conditions ensured the system state was ultimately bounded, with this set contained within another set which approximated the region of attraction. These conditions made the results of [12] applicable to both stable and unstable systems.

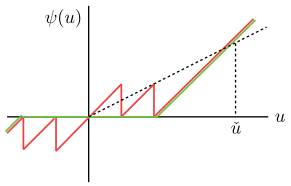

Fig. 1. Issues with sector narrowing with quantization. — $\psi(u) = \mathrm{Dz}(u)$; — $\psi(u) = \pi(u) = u - \mathrm{sat}(q(u))$. When $\psi(u) = \mathrm{Dz}(u)$, then for all $u < \check{u}$, $\psi(u) \in \mathrm{Sector}[0, \varepsilon]$ with $\varepsilon < 1$. When $\psi(u) = \pi(u) = u - \mathrm{sat}(q(u))$, sector narrowing is not possible with the narrowest sector being $\mathrm{Sector}[0, 1]$, regardless of the size of u.

For systems with saturation, it is typical to re-write the saturation nonlinearity as $\mathrm{sat}(u) = u - \mathrm{Dz}(u)$ and then use sector bounds on the deadzone, $\mathrm{Dz}(u)$, to arrive at conditions which ensure stability. These conditions can be stated globally for stable plants, and, by using sector narrowing techniques ([13], [14]), local stability conditions can be obtained for unstable plants. This is not as straightforward for systems suffering from actuator saturation and quantization because the sector narrowing approach cannot be applied. Notice that applying the same split as before yields $\mathrm{sat}(q(u)) = u - \pi(u)$, where the narrowest sector that $\pi(u)$ can inhabit being $\mathrm{Sector}[0, I]$ - see Figure 1. For stable plants this is not problematic, but for unstable plants this effectively prevents any conclusions about stability from being made. Therefore other approaches must be adopted.

An attractive alternative to standard sector constraints for the saturation/quantization nonlinearity can be obtained from the properties of ramp functions which were exploited in the paper [15] (also more recently [16], [17]) for the analysis of piecewise affine systems. Similar to [15], it can be shown that the quantization/saturation nonlinearity can be more accurately approximated by the use of ramp functions, and that such approximations naturally lead to a set of quadratic constraints that can be used in a Lyapunov analysis.

The contribution in this paper is the advocacy of anti-windup compensation (AWC[1]) to address the uniform quantization and saturation problem. AWC is well-studied for systems with input saturation (e.g. [18], [19], [20], [21]) and assists a nominal a priori designed controller during periods of saturation. Although there is some work on applying AWC to input-quantized plants [22], the results developed here go beyond those of [22] where only quantization was considered, and instead use the ultimate-boundedness/local

[1]C.M. Richards is with the Department of Mechanical Engineering, University of Louisville, USA chris.richards@louisville.edu
[2]M.C. Turner is with the School of Electronics and Computer Science, University of Southampton, U.K. m.c.turner@soton.ac.uk
*The material is based upon work supported by the National Science Foundation (Award CMMI-2137030) and the Engineering and Physical Sciences Research Council (Grant number EP/X012654/1).

[1]AWC is used for anti-windup compensat*ion* and anti-windup compensat*or*; the meaning is clear from the context.

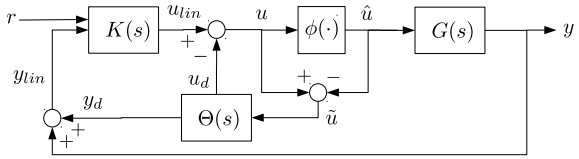

Fig. 2. Configuration of saturated and quantized anti-windup problem: $\phi(u)$ represents the quantized and saturated input; $\Theta(s)$ is the AWC.

stability ideas of [12] along with sharper characterizations of the saturation/quantization nonlinearity, inspired by [15]. This provides less conservative quadratic constraints, and as shown from the results, lower $\mathscr{L}_2$ gain bounds. The approach blends the practicality of the anti-windup approach, the technical rigor of [12] while also reducing conservatism in the design. Crucially, the ramp-function characterizations [15] are exploited for AWC synthesis while only requiring the solution of a linear matrix inequality.

Notation. Let $\mathbb{R}^{n\times m}$ denote the set of matrices with real coefficients of dimension n by m. Let $M_{(i,j)}$ denote the element in the (i,j) entry of matrix M, and M_i the ith row of M, denote $\mathbb{D}^n = \{M \in \mathbb{R}^{n\times n} \mid M_{(i,j)} = 0, i \neq j\}$, $\mathbb{P}^{n\times m} = \{M \in \mathbb{R}^{n\times m} \mid M_{(i,j)} \geq 0, \forall i,j\}$ and $I_n \in \{\mathbb{D}^n \mid I_{n(i,i)} = 1\}$.

II. PROBLEM FORMULATION

A. Quantized and constrained thrust

This paper was inspired by a quantized thrust problem. Consider m thruster banks made up of $n_{T,i}$, $i = 1,\ldots,m$, bidirectional binary thrusters with equal thrust magnitudes δT_i. Then the control signal u is subject to quantization with saturation described by $\phi(u) = \mathrm{sat}_{\bar{u}}(q(u)) = [\ \mathrm{sat}_{\bar{u}_1}(q_1(u_1))\ \ \ldots\ \ \mathrm{sat}_{\bar{u}_m}(q_m(u_m))\ ]'$ where

$$\mathrm{sat}_{\bar{u}_i}(q_i(u_i)) := \begin{cases} -\bar{u}_i & \text{if} \quad q_i(u_i) \leq -\bar{u}_i \\ q_i(u_i) & \text{if} \quad -\bar{u}_i < q_i(u_i) < \bar{u}_i \\ \bar{u}_i, & \text{if} \quad q_i(u_i) \geq \bar{u}_i \end{cases}$$

$$q_i(u_i) := \mathrm{sign}(u_i) \cdot \mathrm{floor}\left(|u_i|/\delta T_i\right) \delta T_i$$

and $\bar{u}_i = n_{T,i}\delta T_i$. Symmetric actuation is assumed throughout; amendments may be made to deal with asymmetric actuators.

B. Anti-windup compensation

The anti-windup architecture shown in Fig. 2 is considered where $G(s)$, $K(s)$, and $\Theta(s)$ are the plant, controller, and AWC, respectively, with state-space realizations:

$$G(s) \sim \begin{cases} \dot{x}_p = A_p x_p + B_p \phi(u) \\ y = C_p x_p \end{cases} \tag{1}$$

$$K(s) \sim \begin{cases} \dot{x}_c = A_c x_c + B_c y_{lin} + B_{cr} r \\ u_{lin} = C_c x_c + D_c y_{lin} + D_{cr} r \end{cases} \tag{2}$$

$$\Theta(s) \sim \begin{cases} \dot{x}_a = (A_p + B_p F) x_a + B_p \tilde{u} \\ u_d = F x_a \\ y_d = C_p x_a \end{cases} \tag{3}$$

where the control signal is $u \in \mathbb{R}^m$, the measured output $y \in \mathbb{R}^p$, and the reference input $r \in \mathbb{R}^{n_r}$. The plant is driven by the quantized and constrained signal $\hat{u} = \phi(u)$ and the AWC is driven by the difference between the control signal and its quantized and constrained counterpart $\tilde{u} = u - \phi(u)$, which will be referred to as the control signal error. The AWC

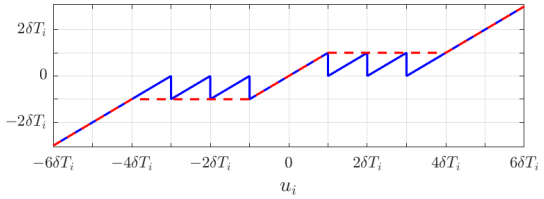

Fig. 3. Bound on control signal error by ramp functions. ___ Control signal error $\tilde{u}_i$; ___ bound $u_i - r_{\delta T_i} + r_{4\delta T_i} + r_{-\delta T_i} - r_{-4\delta T_i} + 3\delta T_i$.

emits two signals, $u_d \in \mathbb{R}^m$ and $y_d \in \mathbb{R}^p$. It is assumed that, in the absence of quantization/saturation, the controller $K(s)$ stabilizes $G(s)$ and provides satisfactory performance.

Remark 1: The quantized and saturated closed-loop system is represented by a set of differential equations with discontinuous right hand side so may not admit classical solutions. In this paper, as in [12], unique Caratheodory solutions are assumed to exist to these differential equations and in this sense the closed-loop is said to be well-posed. Obviously, this excludes sliding mode and other types of behaviour; the interested reader may consult [23] for a general coverage of the subject of discontinuous control systems, or [24] for a differential inclusion formulation.

C. Bound on control signal error

To obtain tighter quadratic constraints than are possible using sector bounds, this paper makes extensive use of ramp functions [15]. The *shifted* ramp function is given by

$$r_{s_i} =: r_i(u_i - s_i) = \begin{cases} 0 & if \quad u_i < s_i \\ u_i - s_i & if \quad u_i \geq s_i \end{cases}, i = 1,\ldots,m$$

The vector-valued decentralized shifted ramp function is

$$r_s =: r(u-s) = [\ r_1(u_1 - s_1)\ \ \ldots\ \ r_m(u_m - s_m)\ ]'$$

For a single thrust control signal, the control signal error $\tilde{u}_i$ is bounded by

$$|\tilde{u}_i| \leq |u_i - r_{\delta T_i} + r_{(n_{T,i}+1)\delta T_i} + r_{-\delta T_i} - r_{-(n_{T_i}+1)\delta T_i} + \bar{u}_i| \tag{4}$$

Fig. 3 illustrates (4) for a thruster bank with 3 thrusters ($n_{T,i} = 3$) with equal thrust magnitudes δT_i. For more compact notation, define $r_{a,i} := r_{\delta T_i}$, $r^-_{a,i} := r_{-\delta T_i}$, $r_{b,i} := r_{(n_{T,i}+1)\delta T_i}$, and $r^-_{b,i} := r_{-(n_{T,i}+1)\delta T_i}$. Then, for $W \in \mathbb{D}^{m\times m} > 0$

$$\tilde{u}' W (u - r_a + r_b + r^-_a - r^-_b + \bar{u} - \tilde{u}) \geq 0 \tag{5}$$

1) Local bound: For unstable or marginally stable systems (the later being pertinent for the rigid body systems considered), it is necessary to confine attention to a region of the state-space surrounding the origin. Notice from Fig. 3 that $|u - r_a + r_b + r^-_a - r^-_b + \bar{u}| - |\tilde{u}| \leq |\delta T|$, $\forall u$. Therefore the following holds

$$\tilde{u}' W (u - r_a + r_b + r^-_a - r^-_b + \bar{u} - \tilde{u} + H x_a) \geq 0 \tag{6}$$

$\forall x_a$ satisfying $\mathrm{sat}_{\delta T}(Hx_a) = Hx_a$. To ensure $\mathrm{sat}_{\delta T}(Hx_a) = Hx_a$, we impose a limit on the energy on the input u_{lin} which drives the AWC (see Fig. 2 and discussion in Section III). If it is true that $\dot{V}(x_a) \leq 2u'_{lin}u_{lin}$ whenever $x'_a P_1 x_a \leq s^2$ and $\|u_{lin}\|_2 \leq s/\sqrt{2}$, $s < 1$, then by integrating $\dot{V}(x_a)$

$$V(x_a) = x'_a P_1 x_a \leq 2\|u_{lin}\|_2^2 \leq s^2$$

Therefore, the following condition is imposed

$$s^2 x_a' H_i' H_i x_a / \delta T_i^2 < x_a' P_1 x_a \tag{7}$$

for all $x_a \neq 0$ and all $i \in \{1,\ldots,m\}$. Thus, when the control signal satisfies the energy condition above and the state remains in the ellipsoid defined by P_1 and s^2, the sector-like bound (6) can be used in the ensuing Lyapunov analysis.

2) Ramp function properties: The shifted ramp function has the following properties:

i) $r_{a,i}(r_{a,i} - (u_i - a_i)) = 0,\ \ i = 1,\ldots,m$. Therefore, for $T_a, T_b \in \mathbb{D}^m$

$$r_a' T_a (r_a - (u-a)) = 0, \quad r_b' T_b (r_b - (u-b)) = 0$$

ii) $(u_i - a_i) - (r_{a,i} - r_{a,i}^-) = 0,\ \ i = 1,\ldots,m$. Therefore, for any $\zeta \in \mathbb{R}^{n_\zeta}$ and $R_a, R_b \in \mathbb{R}^{n_\zeta \times m}$

$$\zeta' R_a (u - a - r_a + r_a^-) = 0, \quad \zeta' R_b (u - b - r_b + r_b^-) = 0$$

iii) $r_{a,i} \geq 0,\ \ r_{a,i}^- \geq 0,\ \ r_{a,i} r_{b,i} \geq 0,\ \ r_{a,i} r_{b,i}^- \geq 0,\ \ r_{a,i}^- r_{b,i}^- \geq 0$ $i = 1,\ldots,m$. Therefore, for $\chi = [\ 1\ r_a'\ r_a^{-\prime}\ r_b'\ r_b^{-\prime}\ ]'$ and $M \in \mathbb{P}^{n_\chi \times n_\chi}$, $n_\chi = 1 + 4m$, $\chi' M \chi \geq 0$.

3) Ultimate boundedness and local attractivity: In the following sections, conditions for ultimate-boundedness of the state and conditions for ensuring the set of ultimate boundedness is itself locally attractive will be given. Therefore, similar to [12], the following sets are introduced:-

$$\mathscr{E}(P_1) = \{x_a \in \mathbb{R}^n; x_a' P_1 x_a \leq 1\},\ P_1 = Q_1^{-1} \tag{8}$$

$$\mathscr{E}(P_2) = \{x_a \in \mathbb{R}^n; x_a' P_2 x_a \leq 1\},\ P_2 = Q_1^{-1} Q_2 Q_1^{-1} \tag{9}$$

where P_1, Q_1, P_2 and Q_2 are positive definite matrices which will be introduced shortly. $\mathscr{E}(P_2)$ represents the set of ultimate boundedness and $\mathscr{E}(P_1)$ represents a larger set such that for all $x_a(0) \in \mathscr{E}(P_1)$, then $x_a(t)$ will converge to a region containing $\mathscr{E}(P_2)$ in finite time.

Remark 2: For unstable plants these sets are necessary to obtain meaningful stability results. For stable plants, they are not necessary, but may improve local performance. □

III. Main Result

A. Linear Performance Recovery

The anti-windup approach proposed in this paper mirrors that of [18] in that conditions are sought to guarantee that the system is "stable" (in the sense discussed in Remark 3 below) and that the mismatch between the ideal linear system, without saturation and quantization, and the real nonlinear system is minimized in some sense. This mismatch system ([18]; see also [25], [14]) is governed by the dynamics:

$$\mathscr{N} \sim \begin{cases} \dot{x}_a &= (A_p + B_p F) x_a + B_p \tilde{u} \\ u &= u_{lin} - F x_a \\ y_d &= C_p x_a \end{cases} \tag{10}$$

where the difference between the ideal linear output y_{lin}, and the actual output y, is y_d. Thus for satisfactory behavior the goal is to synthesize the AWC gain F such that (10) is stable and the $\mathscr{L}_2$ gain from u_{lin} to y_d is bounded by a constant γ.

Remark 3: The reader should understand "stability" in a slightly generalized sense similar to that considered in [12]. In particular, and with some abuse of terminology, $\mathscr{N}$ will be described as stable if, for $u_{lin} \equiv 0$, $x_a(t)$ converges to the smallest level set containing $\mathscr{E}(P_2)$ for all $x_a(0) \in \mathscr{E}(P_1)$ in finite time. Similarly, because $\tilde{u}(t)$ will in general not converge to zero (since the quantization is "active" all the time), a true $\mathscr{L}_2$ gain will, generally, not be possible. Instead, as noted in [22], the $\mathscr{L}_2$-gain-like property enforced is

$$\int_0^T \|y_d(t)\|^2 dt < 2\gamma^2 \int_0^T \|u_{lin}(t)\|^2 dt + \beta \tag{11}$$

for all $T \in [0,\infty)$ and some $\beta > 0$. Despite not being a "true" $\mathscr{L}_2$ gain, it appears minimizing the bound γ is useful. □

B. Stability and performance analysis

Stability, interpreted in the foregoing generalized sense, and performance are guaranteed using quadratic Lyapunov functions and the $\mathscr{L}_2$ gain-like property. The following lemma, assembled from the results of [12], [22] is the starting point for the analysis.

Lemma 1: Consider a dynamic system

$$\mathscr{S} \sim \begin{cases} \dot{x} &= f(x,w) \\ z &= h(x,w) \end{cases} \tag{12}$$

where $f(\cdot,\cdot) : \mathbb{R}^n \times \mathbb{R}^m \mapsto \mathbb{R}^n$ and $h(\cdot,\cdot) : \mathbb{R}^n \times \mathbb{R}^m \mapsto \mathbb{R}^p$ are globally Lipschitz functions. Consider a quadratic Lyapunov function $V(x) = x' P_1 x$, sets $\mathscr{E}(P_1)$, $\mathscr{E}(P_2)$ and scalars τ_1, τ_2 and γ. Assume $P_2 > P_1 > 0$ and $\tau_2 > \tau_1 > 0$, and that the following inequality holds for all $x \neq 0$, $w \neq 0$,

$$\dot{V}(x) + \|z\|^2/\gamma^2 - \|w\|^2 + \tau_1(1 - x' P_1 x) + \tau_2(x' P_2 x - 1) < 0 \tag{13}$$

Then the following are true: 1) when $w = 0$, $\forall x(0) \in \mathscr{E}(P_1)$, the state $x(t)$ converges to the smallest level set containing $\mathscr{E}(P_2)$ in finite time, 2) when w is such that $\|w\|_{2,[0,T]} \leq s/\sqrt{2}$, $s < 1$ and $\|w(t)\|^2 \geq \tau_2 - \tau_1$ for all $t \in [0,T]$, then the following $\mathscr{L}_2$ gain condition holds

$$\int_0^T \|z(t)\|^2 dt < 2\gamma^2 \int_0^T \|w(t)\|^2 dt + \beta \tag{14}$$

Proof: The proof is similar to Lemma 1 in [22], with modifications accounting for the local behavior of the system. 1) When $w = 0$, $x \in \mathscr{E}(P_1)$ and $x \notin \mathscr{E}(P_2)$, inequality (13) implies $\dot{V}(x) < 0$, meaning that the state converges to the smallest level set containing the set $\mathscr{E}(P_2)$. 2) From (13), the assumptions $P_2 > P_1$ and $\tau_2 > \tau_1$ imply $\dot{V}(x) < \|w\|^2 + (\tau_2 - \tau_1)$. Therefore, if $(\tau_2 - \tau_1) \leq \|w\|^2$ on the interval $[0,T]$, $\dot{V}(x) < 2\|w\|^2$ on this interval. Integrating gives $V(x(T)) < s^2$, thus $x(t)$ belongs to the ellipsoid $\mathscr{E}(P_1/s^2)$ over this interval. Since $s < 1$, this implies that, for w satisfying the conditions in the lemma, $x(T) \in \mathscr{E}(P_1)$. Therefore, returning to (13) we have, over the interval $[0,T]$, that $\tau_1(1 - x' P_1 x) \geq 0$ and $x' P_2 x \geq 0$. This implies that

$$\dot{V}(x) + \|z\|^2/\gamma^2 < \|w\|^2 + \tau_2 < 2\|w\|^2 \tag{15}$$

Integrating (15) from $[0,T]$ results in (14). □

The main result is obtained by applying Lemma 1 to system $\mathscr{N}$ and adding the constraints in Section II.C.

Theorem 1: For given scalar $\tau_1 > 0$, if there exist positive definite matrices Q_1, Q_2, a positive definite diagonal matrix U, diagonal matrices T_a, T_b, matrices $R_{a,4}$, L, and positive scalars τ_2, γ such that the linear matrix inequality (18) is

satisfied, then with $F = LQ_1^{-1}$, system (10) is such that: 1) when $u_{lin} = 0$, $\forall x_a(0) \in \mathscr{E}(P_1)$, the state $x_a(t)$ converges to the smallest level set containing $\mathscr{E}(P_2)$ in finite time, 2) when $u_{lin} \neq 0$, the $\mathscr{L}_2$ -like gain condition (11) holds.

Proof: Using the system $\mathscr{N}$ in (10) and the quadratic Lyapunov function $V(x_a) = x_a' P_1 x_a$, inequality (13) becomes

$$\begin{aligned}
&x_a'\big(P_1(A_p+B_pF)+(A_p+B_pF)'P_1\big)x_a + 2x_a'P_1B_p\tilde{u} \\
&\quad + \|y_d\|^2/\gamma - \gamma\|u_{lin}\|^2 + \tau_1(1-x_a'P_1x_a) + \tau_2(x_a'P_2x_a - 1) \\
&\leq x_a'\big(P_1(A_p+B_pF)+(A_p+B_pF)'P_1\big)x_a + 2x_a'P_1B_p\tilde{u} \\
&\quad + \|y_d\|^2/\gamma - \gamma\|u_{lin}\|^2 + \tau_1(1-x_a'P_1x_a) + \tau_2(x_a'P_2x_a - 1) \\
&\quad + 2\tilde{u}'W(u - r_a + r_b + r_a^- - r_b^- + \bar{u} - \tilde{u} + Hx_a) + \chi'M\chi \\
&\quad + 2\chi_a'R_a(u - a - r_a + r_a^-) + 2\chi_b'R_b(u - b - r_b + r_b^-) \\
&\quad + 2r_a'T_a(r_a - (u-a)) + 2r_b'T_b(r_b - (u-b)) < 0 \qquad (16)
\end{aligned}$$

where $\chi_a = [\ 1\ \ x_a'\ \ r_a'\ \ r_a^{-\prime}\ ]'$ and $\chi_b = [\ 1\ \ x_a'\ \ r_b'\ \ r_b^{-\prime}\ ]'$. Partitioning R_a as $R_a = \begin{bmatrix} R_{a,1}' & R_{a,2}' & R_{a,3}' & R_{a,4}' \end{bmatrix}'$ where $R_{a,1} \in \mathbb{R}^{1\times m}$, $R_{a,2} \in \mathbb{R}^{n\times m}$, $R_{a,3}, R_{a,4} \in \mathbb{R}^{m\times m}$. Applying similar partitioning to R_b and partitioning M as $M = \text{block}(M_{ij})$, $i,j = 1,\ldots,5$. Majorizing inequality (16) then leads to the matrix inequality (17). This inequality contains the product of matrix variables which cannot be resolved through standard techniques (e.g., Schur complements or congruence transformations). Therefore, choosing $R_{a,2} = F'R_{a,4}'$, $R_{b,2} = F'R_{b,4}'$, $R_{a,4} = T_a - R_{a,3}$, $R_{b,4} = T_b - R_{b,3}$, $R_{a,1} = -a'R_{a,4}$, $R_{b,1} = -b'R_{b,4}$ and $R_{a,4} = R_{a,4}' = R_{b,4} = R_{b,4}'$. Then, applying a congruence transformation blockdiag$(\ 1,\ P_1^{-1},\ W^{-1},\ R_{a,4}^{-1},\ I,\ \ldots,\ I)$ and Schur complements results in the linear matrix inequality (18) where $U = W^{-1}$, $Z = HQ_1$, $L = FQ_1$, and additional variables are defined in the following remark.

Remark 4: ***i)*** In the (2,2) block element of (18) the nonlinear term $\tau_2 Q_2$ is replaced with Q_2. However, by imposing inequality (19a), then (18) implies (17). ***ii)*** Ensuring $\mathscr{E}(P_2) \subset \mathscr{E}(P_1)$ requires that $x'P_1x \leq x'P_2x \leq 1$ or equivalently, $P_2 - P_1 = Q_1^{-1}Q_2Q_1^{-1} - Q_1^{-1} \geq 0$, which is enforced by (19b). ***iii)*** The (3,4), (4,3), and (10,10) block elements of (18) would contain $R_{a,4}^{-1}$ and the (4,4) block element would contain $-\gamma R_{a,4}^{-2}$. However, these nonlinear block elements are replaced by linear block elements as follows. Define

$$\mathscr{R} := \begin{bmatrix} R_{a,4}^{-1} & R_{a,4}^{-1} \\ * & -\gamma R_{a,4}^{-2} \end{bmatrix} \equiv R_D^{-1}\bar{R}R_D^{-1} < -Y, \quad Y > 0 \quad (20)$$

where $R_D = \text{blockdiag}(R_{a,4},\ R_{a,4})$,

$$\bar{R} = \begin{bmatrix} R_{a,4} & R_{a,4} \\ R_{a,4}' & -\gamma I_m \end{bmatrix}, \quad Y = \begin{bmatrix} Y_{11} & Y_{12} \\ * & Y_{22} \end{bmatrix}$$

and the block elements of Y conform with $\mathscr{R}$. The inequality in (20) is equivalent to (19c), where Young's inequality $-Y^{-1} \leq -2I + Y$ is used in this step [26]. Therefore, by imposing (19c) and replacing the (3,4), (4,3), (4,4), and (10,10) block elements by Y_{12}, Y_{21}, Y_{22}, and Y_{11}, respectively, then (18) implies (17). ***iv)*** Using the Schur complement, inequality (7) is satisfied by (19d). □

To minimize the $\mathscr{L}_2$ gain and increase the region of stability (achieved by maximizing $\mathscr{E}(P_1)$ and the difference in volume between $\mathscr{E}(P_1)$ and $\mathscr{E}(P_2)$) the following optimization is executed with performance weights $\eta_1,\ \eta_2,\ \eta_3$

$$\min\ \eta_1\gamma - \eta_2(|Q_2| - |Q_1|) - \eta_3|Q_1| \quad \text{subject to (18) - (19)}$$

IV. Simulation results

A planetary lander with general architecture shown in Fig. 4 is considered with nonlinear rigid body dynamics given by

$$\dot{x}_p = \left(I_4 \otimes \begin{bmatrix} 0 & 1 \\ 0 & 0 \end{bmatrix}\right) x_p + \left(J_a^{-1} \otimes \begin{bmatrix} 0 \\ 1 \end{bmatrix}\right) T\phi(u) + g(x_p) \otimes \begin{bmatrix} 0 \\ 1 \end{bmatrix} \quad (21)$$

where $x_p = [z\ \dot{z}\ \theta_x\ \dot{\theta}_x\ \theta_y\ \dot{\theta}_y\ \theta_z\ \dot{\theta}_z]'$, $J_a = \text{diag}(m_l,\ J_x,\ J_y,\ J_z)$, $g(x_p)$ is a nonlinear function consisting of cross product terms and an Euler term for the gravitational force, and T is a mapping from thrust to generalized body forces given by

$$T = \begin{bmatrix} -\cos\theta_t & -\cos\theta_t & -\cos\theta_t & -\cos\theta_t \\ -d_y\cos\theta_t & d_y\cos\theta_t & d_y\cos\theta_t & -d_y\cos\theta_t \\ d_x\cos\theta_t & d_x\cos\theta_t & -d_x\cos\theta_t & -d_x\cos\theta_t \\ -\sin\theta_t & \sin\theta_t & -\sin\theta_t & \sin\theta_t \end{bmatrix}$$

The development of these dynamics is described in [20].

As depicted in Fig. 4, each corner of the lander has a thruster bank consisting of three thrusters. The thrusters are unidirectional on/off thrusters, each producing a mass normalized thrust of 0.455 N/kg. The thrusters are tilted slightly toward each corner by a thrust tilt angle θ_t to provide yaw forces. The lander is assumed to operate in the Martian gravitational field ($g = 3.7$ m/s^2). Vehicle parameters are listed in Table I. The required thrust force for hover does not correspond with the available quantized thrust; instead each thruster bank must cycle between two and three thrusters.

TABLE I

Mass normalized landing vehicle parameters

Description	Variable	Value	Unit
mass	m_l	1.0	–
Mass moment of inertia	$[J_x,\ J_y,\ J_z]$	[0.3, 0.3, 0.6]	m^2
Half-spans	$d_x,\ d_y$	2.5	m
Thrust tilt angle	θ_t	2.75	deg

The controller and AWC are designed from the linearized lander dynamics about the hover operating point ($g(x_p) = 0$ in (21)) and it is assumed that all states are measurable, $y = x_p$. Linearization of (21) results in a plant structure: $G(s) = \text{blockdiag}(G_1(s),\ldots,G_4(s))T$. Therefore, following [20], the control signal is taken as $u = T^{-1}(u_{lin} - u_d)$, and the controller and AWC are structured, respectively, as $K(s) = \text{blockdiag}(K_1(s),\ldots,K_4(s))$, $\Theta(s) = \text{blockdiag}(\Theta_1(s),\ldots,\Theta_4(s))T$. Then if $\Theta_i(s)$ is designed, via Theorem 1, to stabilize the ith plant-controller combination, the diagonally structured system is asymptotically stable.

Each $K_i(s)$ implements full-state feedback control with reference tracking: $K_i(s) \sim \{\dot{x}_c = -C_r y_{lin} + r,\ u_{lin} = K_I x_c + K_x y_{lin}$, where $C_r = [1\ \ 0]$ such that $z_p = [z\ \ \theta_x\ \ \theta_y\ \ \theta_z]'$ are the tracked states, and K_I and K_x are integral and full-state feedback gains, respectively, designed such that the nominal closed-loop system poles lie at $[-1,\ -1.5,\ -2]$ for each channel. The design parameters of each $\Theta_i(s)$ are $\tau_1 = 0.99$, $s = 1/25$, $\eta = \tilde{\eta}/\sum\tilde{\eta}$ where $\tilde{\eta} = [5\ 300\ 200]$, which result in $\gamma = (48,\ 520,\ 520,\ 141)$ for each channel. For comparison, a Sector[0,1] calculation – performed by solving an LMI representing the terms left of the non-strict inequality

$$\begin{bmatrix}
\mathscr{M}_{11} & \mathscr{M}_{12} & \bar{u}' & R_{a,1}+R_{b,1} & M_{12}-R_{a,1}+a'T_a-a'R'_{a,3} & M_{13}+R_{a,1}-a'R'_{a,4} & M_{14}+b'T_b-R_{b,1}-b'R'_{b,3} & M_{15}+R_{b,1}-b'R'_{b,4} \\
* & \mathscr{M}_{22} & P_1B_p-F'W+H'W & R_{a,2}+R_{b,2} & F'T_a-R_{a,2}-F'R'_{a,3} & R_{a,2}-F'R'_{a,4} & F'T_b-R_{b,2}-F'R'_{b,3} & R_{b,2}-F'R'_{b,4} \\
* & * & -2\bar{W} & \bar{W} & -\bar{W} & \bar{W} & \bar{W} & -\bar{W} \\
* & * & * & -\gamma I & R'_{a,3}-T_a & R'_{a,4} & R'_{b,3}-T_b & R'_{b,4} \\
* & * & * & * & M_{22}+2T_a-2R_{a,3} & M_{23}+R_{a,3}-R'_{a,4} & M_{24} & M_{25} \\
* & * & * & * & * & M_{33}+2R_{a,4} & M_{34} & M_{35} \\
* & * & * & * & * & * & M_{44}+2T_b-2R_{b,3} & M_{45}+R_{b,3}-R'_{b,4} \\
* & * & * & * & * & * & * & M_{55}+2R_{b,4}
\end{bmatrix} < 0 \quad (17)$$

$$\mathscr{M}_{11} = M_{11} - 2R_{a,1}a - 2R_{b,1}b + \tau_1 - \tau_2, \quad \mathscr{M}_{12} = -R_{a,1}F - R_{b,1}F - a'R'_{a,2} - b'R'_{b,2}$$

$$\mathscr{M}_{22} = P_1(A_p + B_pF) + (A_p + B_pF)'P_1 + \frac{1}{\gamma}C'_pC_p - (R_{a,2}+R_{b,2})F - F'(R_{a,2}+R_{b,2})' - \tau_1 P_1 + \tau_2 P_2$$

$$\begin{bmatrix}
\mathscr{M}_{11} & 0 & \bar{u}'U & -a'-b' & M_{12}+2a'R_{a,4} & M_{13}-2a'R_{a,4} & M_{14}+2b'R_{a,4} & M_{15}-2b'R_{a,4} & 0 & 0 \\
* & \mathscr{M}_{22} & B_pU-L'+Z' & 2L' & 0 & 0 & 0 & 0 & Q_1C'_p & 2L' \\
* & * & -2U & Y_{12} & -I & I & I & -I & 0 & 0 \\
* & * & * & Y_{22} & -I & I & -I & I & 0 & 0 \\
* & * & * & * & M_{22}+2R_{a,4} & M_{23}+T_a-2R_{a,4} & M_{24} & M_{25} & 0 & 0 \\
* & * & * & * & * & M_{33}+2R_{a,4} & M_{34} & M_{35} & 0 & 0 \\
* & * & * & * & * & * & M_{44}+2R_{a,4} & M_{45}+T_b-2R_{a,4} & 0 & 0 \\
* & * & * & * & * & * & * & M_{55}+2R_{a,4} & 0 & 0 \\
* & * & * & * & * & * & * & * & -\gamma I & 0 \\
* & * & * & * & * & * & * & * & * & Y_{11}
\end{bmatrix} < 0 \quad (18)$$

$$\mathscr{M}_{11} = M_{11} + 2a'R_{a,4}a + 2b'R_{a,4}b + \tau_1 - \tau_2, \qquad \mathscr{M}_{22} = A_pQ_1 + B_pL + Q_1A'_p + L'B'_p - \tau_1 Q_1 + Q_2$$

$$\tau_2 < 1 \quad \text{(a)}, \qquad Q_1 < Q_2 \quad \text{(b)}, \qquad \begin{bmatrix} \bar{R} & R_D \\ R_D & -2I_{2m}+Y \end{bmatrix} < 0 \quad \text{(c)}, \qquad \begin{bmatrix} Q_1 & Z'_i \\ Z_i & \delta T_i^2/s^2 \end{bmatrix} > 0 \quad \forall i \in \{1,2,\ldots,m\} \quad \text{(d)} \qquad (19)$$

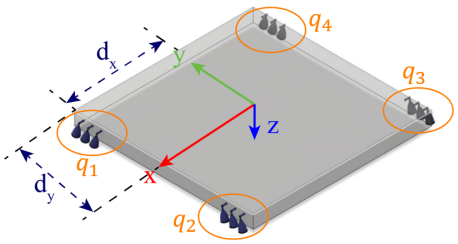

Fig. 4. General architecture of a planetary lander.

in (16) along with (19a,b,d) – gives: $\gamma = (1,\ 13,\ 13,\ 3)\times 10^6$. From this, we see that the less conservative ramp functions constrains yield much lower $\mathscr{L}_2$ gain bounds.

The design parameters described above are used for the simulations and $K(s)$ remains the same with and without AWC. Also, the simulations include the full nonlinear dynamics (21). Fig. 5 shows the response to a reference commanding the vehicle to decrease in altitude and roll about the x-axis. Without AWC the vehicle is unable to follow the reference and the thrust remains saturated after 9 seconds (similar results are seen with the other thruster banks). With AWC the vehicle is able to follow the reference (noting the slowest closed-loop time constant is 1 second) and the thruster bank cycles between 2-to-3 thrusters upon reaching steady state. This is the appropriate cycling for hover.

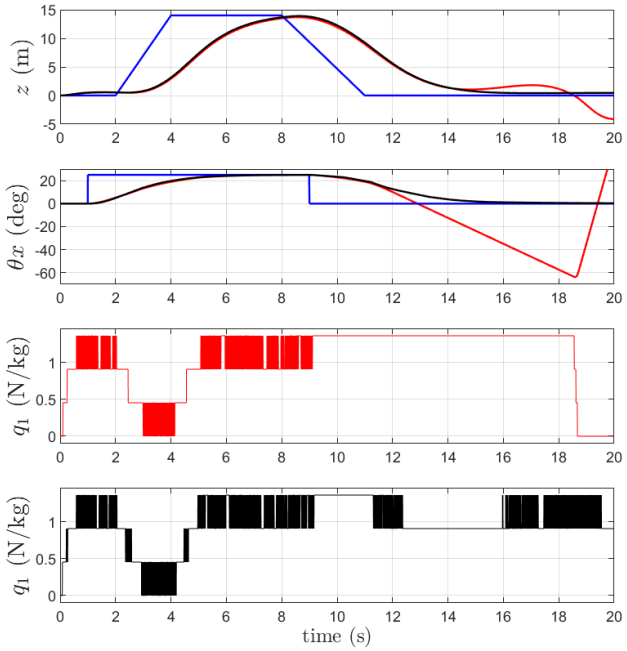

Fig. 5. Lander with three thrusters per thruster bank: response to reference input. Reference; without anti-windup; with anti-windup.

To emphasize the AWC capability for managing quantization, the number of thrusters per thruster bank is increased

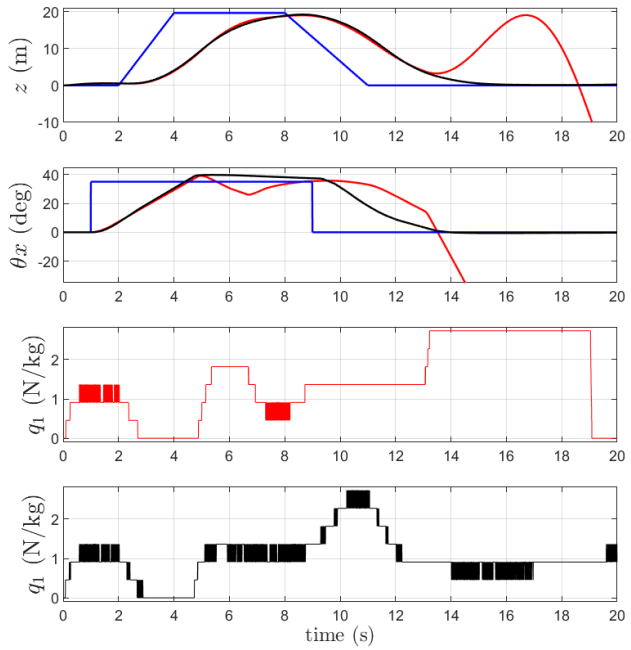

Fig. 6. Lander with six thrusters per thruster bank: response to reference input. Reference; without anti-windup; with anti-windup.

to 6. Fig. 6 illustrates the response to reference commands similar to the prior case. While the thrust without AWC is able to remain with in the saturation limits during the first 12 seconds, it is unable to adjust accordingly to maintain hover after the (dynamic or non-hovering) reference commands have ended. As a result the thrust saturates and the vehicle diverges from hover. With AWC, the thrust only reaches the saturation limit for a brief period once the dynamic reference commands have ended and returns within the limits cycling between the appropriate levels to maintain hover.

Remark 5: Simulations with the lander dynamics linearized about the hover operating point ($g(x_p) = 0$ in (21)) were executed but are not shown due to space restrictions. Results similar to those presented occur when the reference commands are increased in magnitude by 50% and 93% for the lander with 3 and 6 thrusters per thruster bank, respectively. For reference commands below these magnitudes, the linearized lander with and without AWC are able to recover.

V. CONCLUSIONS

An anti-windup design method for systems subject to input quantization/saturation has been developed. Salient features of the work are: the AWC synthesis conditions are framed as LMIs; ramp functions have been exploited to obtain sharper results than available through standard sector analysis; and the results are applicable to rigid body systems, which motivated the work. This approach has transferability to many non-traditional control problems (e.g., drug delivery, often inherently quantized; environmental management, often quota-based) as well as traditional control fields where quantization is intrinsic (network control, communications, event-triggered control systems). Future work will explore extensions that address issues resulting from finite rate of switching. Simultaneous controller and AWC design will also be investigated as a potential to enlarge the region of stability.

REFERENCES

[1] R. W. Brockett and D. Liberzon, "Quantized feedback stabilization of linear systems," IEEE Trans. Automat. Cont., vol. 45, no. 7, pp. 1279–1289, 2000.

[2] J. Orphee, M. Hannan, E. Braden, E. Anzalone, N. Ahmed, S. Craig, N. Olson, J. Everett, and K. Miller, "Guidance, navigation, & control for NASA lunar pallet lander," in American Astronautical Society Annual Guidance, Navigation & Control Conf., 2019, pp. 117–128.

[3] D. F. Delchamps, "Stabilizing a linear system with quantized state feedback," IEEE Trans. Automat. Cont., vol. 35, no. 8, pp. 916–924, 1990.

[4] S. Azuma and T. Sugie, "Synthesis of optimal dynamic quantizers for discrete-valued input control," IEEE Trans. Automat. Cont., vol. 53, no. 9, pp. 2064–2075, 2008.

[5] ——, "Stability analysis of quantized feedback systems including optimal dynamic quantizers," in Conf. on Dec. and Cont., 2008, pp. 3392–3397.

[6] J. M. Gonçalves, A. Megretski, and M. A. Dahleh, "Global stability of relay feedback systems," IEEE Trans. Automat. Cont., vol. 46, no. 4, pp. 550–562, 2001.

[7] K. Ahn and S. Yokota, "Intelligent switching control of pneumatic actuator using on/off solenoid valves," Mechatronics, vol. 15, no. 6, pp. 683–702, 2005.

[8] R. Kalman, "Nonlinear aspects of sampled-data control systems," in Proc. Symp. Nonlinear Circuit Analysis VI, 1956, 1956, pp. 273–313.

[9] F. Bullo and D. Liberzon, "Quantized control via locational optimization," IEEE Trans. Automat. Cont., vol. 51, no. 1, pp. 2–13, 2006.

[10] M. Fu and L. Xie, "The sector bound approach to quantized feedback control," IEEE Trans. Automat. Cont., vol. 50, no. 11, pp. 1698–1711, 2005.

[11] N. Elia and S. K. Mitter, "Stabilization of linear systems with limited information," IEEE Trans. Automat. Cont., vol. 46, no. 9, pp. 1384–1400, 2001.

[12] S. Tarbouriech and F. Gouaisbaut, "Control design for quantized linear systems with saturations," IEEE Trans. Automat. Cont., vol. 57, no. 7, pp. 1883–1889, 2011.

[13] H. Hindi and S. Boyd, "Analysis of linear systems with saturation using convex optimization," in Conf. on Dec. and Cont., vol. 1, 1998, pp. 903–908.

[14] L. Zaccarian and A. R. Teel, Modern anti-windup synthesis: control augmentation for actuator saturation. Princeton University Press, 2011, vol. 36.

[15] L. Groff, G. Valmorbida, and J. Gomes da Silva, "Stability analysis for piecewise affine discrete-time systems," in Conf. on Dec. and Cont. IEEE, 2019, pp. 8172–8177.

[16] G. Valmorbida and F. Ferrante, "On quantization in discrete-time control systems: Stability analysis of ternary controllers," in Conf. on Dec. and Cont. IEEE, 2020, pp. 2543–2548.

[17] F. Ferrante and G. Valmorbida, "Stability analysis of a class of discontinuous discrete-time systems," IEEE Control Systems Letters, vol. 7, pp. 454–459, 2023.

[18] M. C. Turner, G. Herrmann, and I. Postlethwaite, "Incorporating robustness requirements into antiwindup design," IEEE Trans. Automat. Cont., vol. 52, no. 10, pp. 1842–1855, 2007.

[19] E. F. Mulder, M. V. Kothare, and M. Morari, "Multivariable anti-windup controller synthesis using linear matrix inequalities," Automatica, vol. 37, no. 9, pp. 1407–1416, 2001.

[20] C. M. Richards and M. C. Turner, "Combined static and dynamic anti-windup compensation for quadcopters experiencing large disturbances," Journal of Guidance, Control, and Navigation, vol. 43, no. 4, pp. 673–684, 2020.

[21] D. S. Bernstein and A. N. Michel, "A chronological bibliography on saturating actuators," Int. J. Robust Nonlinear Control, vol. 5, no. 5, pp. 375–380, 1995.

[22] J. Sofrony and M. Turner, "Anti-windup design for systems with input quantization," in Conf. on Dec. and Cont., 2015, pp. 7586–7591.

[23] J. Cortes, "Discontinuous dynamical systems," IEEE Control Syst. Mag., vol. 28, no. 3, pp. 36–73, 2008.

[24] T. Hu and Z. Lin, Control systems with actuator saturation: analysis and design. Birkhäuser, 2001.

[25] A. R. Teel and N. Kapoor, "The $\mathscr{L}_2$ anti-windup problem: Its definition and solution," in European Control Conference, 1997, pp. 1897–1902.

[26] R. J. Caverly and J. R. Forbes, "LMI properties and applications in systems, stability, and control theory," 2019. [Online]. Available: https://arxiv.org/abs/1903.08599